Letters
IOP Publishing
Smart Materials and Structures
Smart Mater. Struct. 29 (2020) 04LT01 (5pp)
https://doi.org/10.1088/1361-665X/ab7543

Letter

New insight into piezoelectric energy harvesting with mechanical and electrical nonlinearities

Jiahua Wang[1], Bao Zhao[2], Wei-Hsin Liao[1] and Junrui Liang[2]

[1] Department of Mechanical and Automation Engineering, The Chinese University of Hong Kong, Shatin, NT, Hong Kong, People's Republic of China
[2] School of Information Science and Technology, ShanghaiTech University, No. 393, Middle Huaxia Road, Pudong, Shanghai 201210, People's Republic of China

E-mail: whliao@cuhk.edu.hk

Received 4 November 2019, revised 12 January 2020
Accepted for publication 11 February 2020
Published 27 February 2020

Abstract

This letter investigates the piezoelectric energy harvesting system with mechanical and electrical nonlinearities. Through impedance model, nonlinear interface circuits for energy harvesting purpose can be simplified as an electrical impedance with real and imaginary parts. Their effects on the mechanical structure can be regarded as circuit-induced damping and stiffness. The resulted equivalent mechanical vibratory system allows us to analytically obtain the system responses under different excitation and loading conditions by harmonic balance method. Furthermore, it becomes possible to achieve a comprehensive comparison among different nonlinear interface circuits, including the standard energy harvesting circuit, synchronized electric charge extraction circuit, series synchronized switching on inductor circuit, parallel synchronized switching on inductor circuit and parallel synchronized triple bias-flip circuit. The results from the theoretical model and experiments together reveal that the nonlinearities play a significant role in the energy harvester's hysteresis region size, displacement amplitude, and piezoelectric voltage level. This investigation provides an insight into the design, optimization and implementation for the nonlinear energy harvester.

Keywords: nonlinear interface circuit, nonlinear energy harvester, harmonic balance method, impedance model

(Some figures may appear in colour only in the online journal)

Introduction

The piezoelectric energy harvester has been deemed as a potential solution for power shortage and battery maintenance problems in WSNs due to its scalability and simplicity [1]. It generally consists of a mechanical transformer, a piezoelectric transducer, and an interface circuit. In decades' developments, regarding these three parts, different system enhancement strategies have been proposed. Firstly, the frequency-tuning technique [2], multi-modal configuration [3], frequency-up conversion [4, 5] and nonlinear design [6, 7] have been employed to amplify the mechanical excitation input. It was shown that the nonlinear piezoelectric energy harvester with a purely resistive load offers a broader bandwidth [7]. In addition, advancements in piezoelectric materials contribute to a high electromechanical coupling effect, which improves the energy conversion efficiency between the mechanical domain and electrical domain [8, 9]. Finally, nonlinear interface circuits involving charge manipulation can extract more net energy from the source by increasing the positive work as the product of voltage and current. The most studied circuit solutions include standard energy harvesting

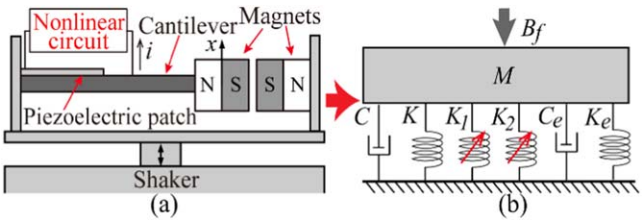

Figure 1. The nonlinear energy harvester with a nonlinear circuit (a) system overview; (b) equivalent lumped parameter model.

circuit (SEH), synchronized electric charge extraction circuit (SECE), series synchronized switching on inductor circuit (S-SSHI), parallel synchronized switching on inductor circuit (P-SSHI), and parallel synchronized triple bias-flip circuit (P-S3BF). Researches have revealed that nonlinear interface circuit solutions, as connected with a linear energy harvester, could obtain multifold output gain [10]. It is interesting to investigate how these strategies play jointly.

Neglecting material differences, researchers have explored mutual influences of the nonlinear mechanical transformer with nonlinear interface circuit. Chen *et al* [11] employed SIMULINK and PSIM to simulate a bistable energy harvester with SEH and S-SSHI. Their results showed the bistable energy harvester with S-SSHI provided higher power output generally, while little attention had been paid to the bandwidth characteristic. Similarly, Singh *et al* [12] concluded that nonlinear energy harvester contributed to larger vibration amplitude and frequency spectrum, compared with the linear system on SEH, SECE, and P-SSHI. Comparisons between SEH and purely resistive AC circuit were made in [13, 14]. Results showed that SEH diminished power level and bandwidth due to the increased damping. Dai and Harne explored the effects of combined harmonic and stochastic excitations on a bistable energy harvester with SEH [15]. The interaction between the bistable energy harvester and SEH was not treated. Cai and Harne optimized the power of a bistable transformer with a diode bridge and a buck-boost converter [16]. P-SSHI and SEH's effects on the bandwidth and power level of monostable energy harvester were studied through simulation in SIMULINK [17]. Huguet *et al* [18] explored the bistable energy harvester with SECE circuit.

From the previous literature, it is concluded that an efficient modeling method and a comparative insight for different circuit solutions with a nonlinear transformer are still missing. To facilitate the energy harvesting system design, optimization and implementation, this paper aims to analytically derive the closed-form solutions of SEH, SECE, S-SSHI, P-SSHI and P-S3BF with a monostable energy harvester through impedance model and harmonic balance method. Systems' hysteresis region, vibration amplitude, and voltage level will be discussed.

Modeling

A schematic nonlinear piezoelectric energy harvester is connected with nonlinear energy harvesting interface circuits, as shown in figure 1(a). The monostable nonlinearity is obtained through repelling forces of two magnets. The lumped parameter model is adopted, and the constitutive equations can be

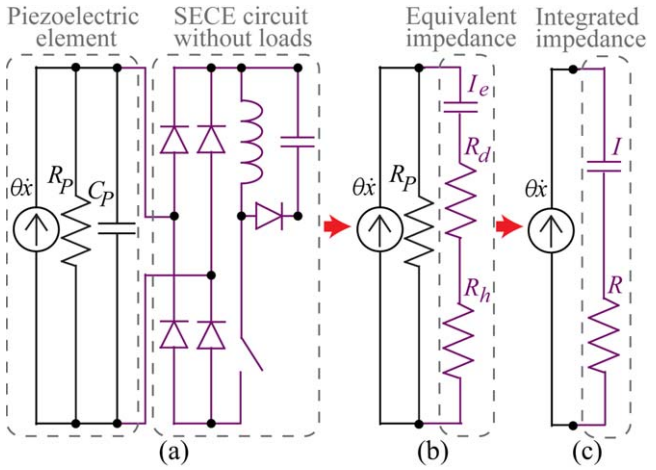

Figure 2. Equivalent circuit model (a) equivalent piezoelectric element connected with SECE without loads, (b) equivalent impedance, (c) integrated impedance.

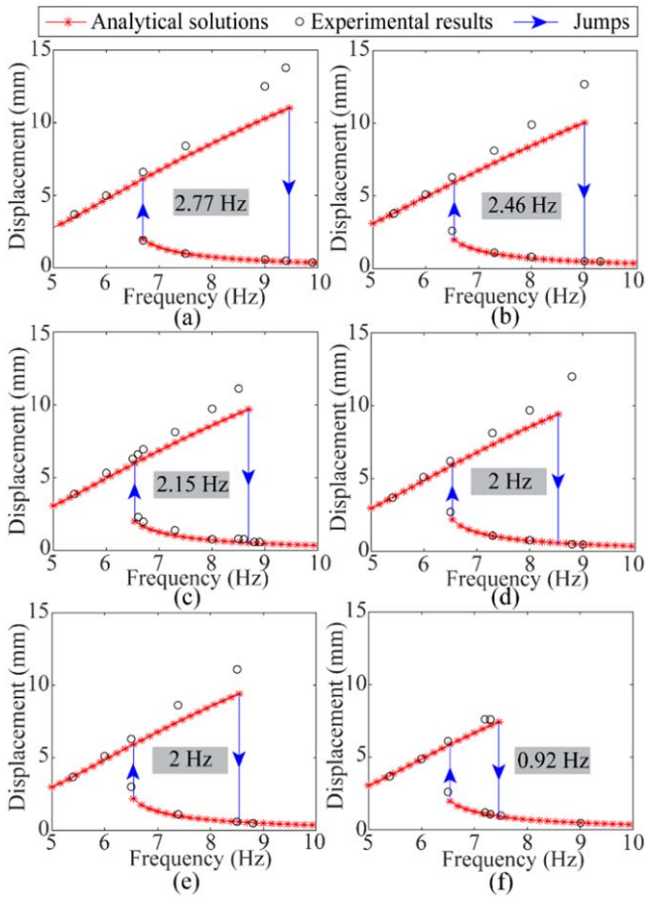

Figure 3. Frequency response of the monostable transformer connected with different nonlinear circuits. Red stars denote analytical solutions, while experimental results are marked by circles. The blue arrows define the jumps and hysteresis region size is highlighted by shading. (a) Pure mechanical structure, (b) SEH, (c) SECE, (d) S-SSHI, (e) P-SSHI, (f) P-S3BF.

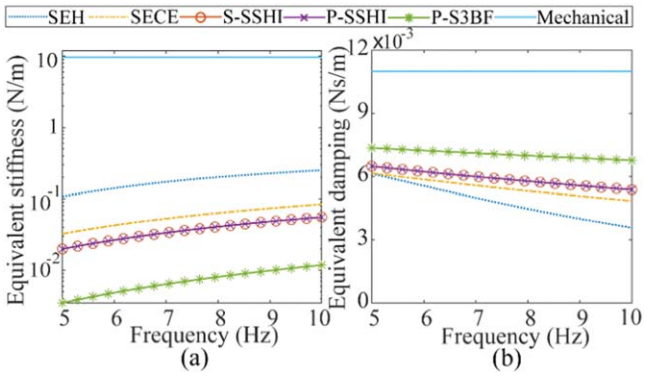

Figure 4. The circuit-induced stiffness and damping compared with mechanical stiffness and damping. (a) equivalent stiffness, (b) equivalent damping

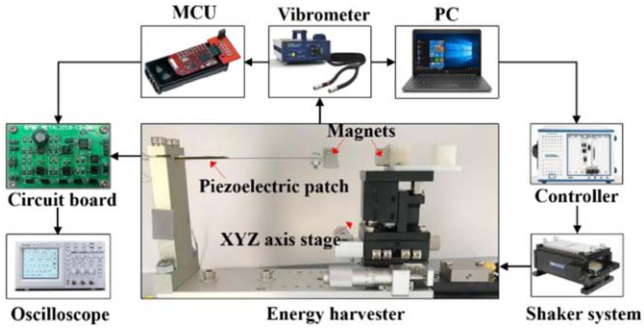

Figure 5. Experimental setup.

Table 1. System parameters.

Parameters	Value	Parameters	Value
M (g)	8.61	θ (mN V^{-1})	0.127
C (Ns m^{-1})	0.011	B_f (mN)	8.61
K (N m^{-1})	51.15	C_P (nF)	35.61
K_1 (N m^{-1})	−41.44	R_P (KΩ)	503
K_2 (kN m^{-3})	231.16	γ	−0.20

represented as [6, 19]

$$M\ddot{x} + C\dot{x} + Kx + K_1x + K_2x^3 + \theta v = B_f\cos\omega t, \quad (1)$$

$$\theta\dot{x} - \frac{v}{R_P} - C_P\dot{v} - i = 0, \quad (2)$$

where M, C, K denote equivalent mass, damping, and stiffness, while K_1, K_2 are the linear and nonlinear stiffness caused by magnets, which can be obtained through the dipole–dipole model [20]. The electromechanical coupling coefficient is marked by θ. B_f and ω are the harmonic base excitation amplitude and frequency. R_P and C_P are the parasitic resistance and clamped capacitance of the piezoelectric element. The displacement of the equivalent mass and voltage of the piezoelectric element are denoted as x and v. i represents the current going through the nonlinear interface circuit.

This work deals with nonlinear SEH, SECE, S-SSHI, P-SSHI and P-S3BF circuits. Taking the SECE circuit as an example, we derive the system dynamics when connected with a monostable energy harvester. Neglecting the load, the piezoelectric element and connected SECE circuit can be equalized as a current source in parallel with a parasitic resistance R_P and an equivalent impedance. The equivalent impedance, shown in figure 2, consists of a vibratory component I_e, dissipative component R_d, and harvesting component R_h [21] yielding

$$R_h = \frac{4|\gamma|}{\pi\omega C_p},\ R_d = \frac{4(1+\gamma)}{\pi\omega C_p},\ I_e = -\frac{1}{\omega C_p}. \quad (3)$$

The equivalent impedance in parallel with R_P leads to an integrated impedance $Z = R + jI$ with a real part R and an imaginary part I

$$R = \frac{R_P(4R_P\pi\omega C_p + \pi^2 + 16)}{C_P^2\pi^2R_P^2\omega^2 + 8R_P\pi\omega C_p + \pi^2 + 16}, \quad (4)$$

$$I = -\frac{R_P^2C_p\omega\pi^2}{C_P^2\pi^2R_P^2\omega^2 + 8R_P\pi\omega C_p + \pi^2 + 16}, \quad (5)$$

where j is the imaginary symbol. With the electromechanical analogy, the effects of the circuit on the mechanical oscillator can be equalized as equivalent dissipative damping C_e and electrically induced stiffness K_e [22]

$$C_e = \theta^2R,\ K_e = -\theta^2\omega I. \quad (6)$$

Thus, the electromechanical system can be simplified as a pure mechanical oscillator, as shown in figure 1(b). The system can be represented as

$$M\ddot{x} + C\dot{x} + Kx + K_1x + K_2x^3 + C_e\dot{x} + K_ex = B_f\cos\omega t. \quad (7)$$

Using harmonic balance method, we assume the steady motion of the oscillator as first-order harmonic of

$$x = a\cdot\cos(\omega t) + b\cdot\sin(\omega t), \quad (8)$$

where a and b are time-invariant coefficients. Substituting the assumption into equation (7), and equalizing coefficients of $\sin(\omega t)$ and $\cos(\omega t)$ terms, a six-ordered formula about steady-state vibration amplitude $X = \sqrt{a^2 + b^2}$ can be obtained as

$$\left(\left(C\omega + \frac{\theta^2R_P(4R_P\pi\omega C_p + \pi^2 + 16)\omega}{C_P^2\pi^2R_P^2\omega^2 + 8R_P\pi\omega C_p + \pi^2 + 16}\right)^2 + (-M\omega^2 + K - K_1 + \times\frac{\theta^2R_P^2\omega^2C_p\pi^2}{C_P^2\pi^2R_P^2\omega^2 + 8R_P\pi\omega C_p + \pi^2 + 16} + \frac{3K_2X^2}{4}\right)^2\right)X^2 = B_f^2. \quad (9)$$

Solving the equation gives the relationship between external excitation and system responses. Following the same procedure, the monostable piezoelectric energy harvester connected with other nonlinear circuits is also studied. This closed-form

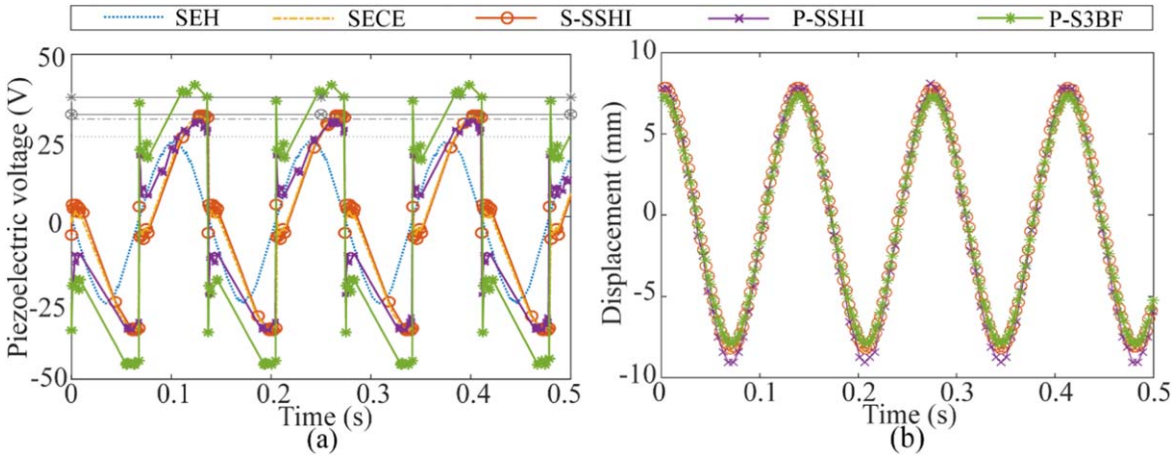

Figure 6. Experimental capture of piezoelectric voltage and mass displacement, (a) piezoelectric voltage history, the grey curves are analytically solved voltage amplitude, (b) displacement history.

solution can facilitate system design, optimization, and implementation.

The results are plotted in figure 3. For one thing, the sole monostable transformer without circuits has the largest displacement hysteresis region of 2.77 Hz from 6.7 Hz to 9.47 Hz. Without effects of circuits, the displacement amplitude peak can reach as high as 12 mm in simulation. As there is a nonlinear circuit, both the system's hysteresis region size and vibration amplitude are compressed. As shown in figure 4, the nonlinear circuit tunes the stiffness and damping of the oscillator, and the damping effect dominates since its value is commensurate with the mechanical damping. It is revealed that the P-S3BF causes the largest damping. The S-SSHI and P-SSHI introduce the same resistance into the system, followed by the SECE. The resulted bandwidth and vibration amplitude are similar for these three circuits. The findings are consistent with conclusions in [10]. As a result, the bandwidth and amplitude of the oscillator decrease further for the circuits in the very order as listed in figure 3.

For another, the voltage level on the piezoelectric transducer is also a concern as it is related to the output power. From figure 2(c), according to Kirchhoff's circuit law, the piezoelectric voltage can be attained as

$$V = \theta\dot{x} \times Z_m e^{j\vartheta}, \tag{10}$$

where $Z_m = \sqrt{R^2 + I^2}$, $\vartheta = \arctan(I/R)$, yielding the voltage amplitude

$$V_{amp} = \theta\omega X Z_m, \tag{11}$$

It can be shown that both the vibration amplitude and impedance magnitude account for the voltage amplitude. A large impedance suppresses the vibration, while it may also compensate for the displacement loss to produce a high voltage.

Experiments and results

An experiment has been set up as shown in figure 5. For the same monostable energy harvester, different circuits on a PCB board are connected and tested. A vibration system is used to control base excitation to the energy harvester. The vibrometer and oscilloscope are used to track system vibration and piezoelectric voltage, respectively. For switch control in SECE, S-SSHI, P-SSHI, and P-S3BF, the switch action with a flip factor γ is controlled by an MCU (MSP430 F2274) based on the velocity signal from the vibrometer. The measured system parameters are summarized in table 1.

The experimental displacement response has been plotted in figure 3 denoted by circles. The suppression effects of different circuits on the mechanical oscillator are observed and similar to the previous interpretations. As the displacement increases, the error between model and experiments seems to build up. The reason is that the rotation of the beam end would introduce measurement error by the vibrometer at large deflection. The general consistency between experiments and analytical solutions validates the proposed model for integration of the monostable energy harvester and nonlinear circuits. To quantify the piezoelectric voltage, next, the piezoelectric voltage and displacement histories at 7.3 Hz base excitation for each circuit are displayed in figure 6. The predicted voltage amplitude is also shown by grey curves, which is consistent with experimental results. It is observed that the SEH circuit outputs the lowest voltage, while the P-S3BF realizes the highest voltage around 40 V. It demonstrates that the strong impedance may enhance the voltage level as equation (11) indicates. This reminds us that trade-off between the hysteresis region and voltage level should be taken care. For example, under wide-band excitations, the voltage level may be sacrificed for more robust implementation when choosing SEH. The proposed modeling method sheds light on circuit choice for particular applications.

Conclusions

In summary, this letter has modeled the monostable piezoelectric energy harvester with different nonlinear circuits, including SEH, SECE, S-SSHI, P-SSHI, and P-S3BF. Using

impedance model and harmonic balance method, the system responses have been analytically obtained. Results showed that the hysteresis region and displacement amplitude were compressed as the nonlinear circuit appeared, while for different circuits, the suppression strength varied. The analysis and simulation results were validated by experiments. The comprehensive insight on monostable energy harvester with nonlinear circuits provided us instructions on the design of nonlinear energy harvesters. Through comparison among various circuits, a balance between the bandwidth and voltage level should be considered for specific applications. This work inspires us that a system-level design, optimization and implementation for energy harvester development is needed. Overall optimization, empowered by the proposed modeling method, covering mechanical and electrical aspects will be addressed in the future.

Acknowledgments

This work was supported by Research Grants Council of Hong Kong Special Administrative Region, China (Project No. CUHK 14205917); and National Natural Science Foundation of China (Project No. 61401277), ShanghaiTech University (Project No. F-0203-13-003). The support for Mr Jiahua Wang provided by Research Grants Council under Hong Kong PhD Fellowship Scheme is also acknowledged.

ORCID iDs

Wei-Hsin Liao https://orcid.org/0000-0001-7221-5906
Junrui Liang https://orcid.org/0000-0003-2685-5587

References

[1] Safaei M, Sodano H A and Anton S R 2019 *Smart Mater. Struct.* **28** 113001
[2] Staaf L G H, Smith A D, Köhler E, Lundgren P, Folkow P D and Enoksson P 2018 *J. Sound Vib.* **420** 165
[3] Toyabur R M, Salauddin M, Cho H and Park J Y 2018 *Energy Convers. Manage.* **168** 454
[4] Fu X and Liao W-H 2019 *J. Vib. Acoust.* **141** 031002
[5] Chen J and Wang Y 2019 *Appl. Phys. Lett.* **114** 053902
[6] Wang J and Liao W-H 2019 *Energy Convers. Manage.* **192** 30
[7] Yang Z, Tang L, Tao K and Aw K 2019 *Smart Mater. Struct.* **28** 10LT02
[8] Sappati K and Bhadra S 2018 *Sensors* **18** 3605
[9] Gui J, Zhu Y, Zhang L, Shu X, Liu W, Guo S and Zhao X 2018 *Appl. Phys. Lett.* **112** 072902
[10] Liang J, Zhao Y and Zhao K 2018 *IEEE Trans. Power Electron.* **34** 275
[11] Chen Y-Y, Vasic D, Liu Y-P and Costa F 2013 *J. Intell. Mater. Syst. Struct.* **24** 180
[12] Singh K A, Kumar R and Weber R J 2015 *IEEE Trans. Power Electron.* **30** 6763
[13] Tang L, Han Y, Hand J and Harne R L 2016 *Proc. SPIE* **9799** 97990J
[14] Lan C, Tang L and Harne R L 2018 *J. Sound Vib.* **421** 61
[15] Quanqi Dai and Harne R L 2018 *J. Intell. Mater. Syst. Struct.* **29** 514
[16] Cai W and Harne R L 2018 *J. Intell. Mater. Syst. Struct.* **30** 213
[17] Silva T, Tan D, Marqui C D and Erturk A 2019 *J. Intell. Mater. Syst. Struct.* **30** 965
[18] Huguet T, Lallart M and Badel A 2019 *Nonlinear Dyn.* **97** 485
[19] Rezaei M, Talebitooti R and Friswell M I 2019 *Smart Mater. Struct.* **28** 105037
[20] Zou H-X, Zhang W-M, Wei K-X, Li W-B, Peng Z-K and Meng G 2016 *J. Appl. Mech.* **83** 121005
[21] Chen C, Zhao B and Liang J 2019 *Smart Mater. Struct.* **28** 105053
[22] Liang J and Liao W-H 2012 *IEEE/ASME Trans. Mechatron.* **17** 1145